JGR Space Physics

RESEARCH ARTICLE
10.1029/2019JA027493

Effects of IMF By on Ring Current Asymmetry Under Southward IMF Bz Conditions Observed at Ground Magnetic Stations: Case Studies

Sandeep Kumar[1,2], B. Veenadhari[3], D. Chakrabarty[1], S. Tulasi Ram[3], T. Kikuchi[4], and Y. Miyoshi[2]

[1]Space and Atmospheric Sciences Division, Physical Research Laboratory, Navrangpura, Ahmedabad, India, [2]Institute for Space-Earth Environmental Research, Nagoya University, Nagoya, Japan, [3]Indian Institute of Geomagnetism, Navi Mumbai, India, [4]Research Institute for Sustainable Humanosphere, Kyoto University, Uji, Japan

Key Points:
- IMF By plays important role in asymmetry of the ring current observed at ground stations in addition to IMF Bz
- SuperDARN convection cells and AMPERE-derived FACs show the association of IMF By with MLT distribution of the ring current
- Under suitable conditions, IMF By can alter the MLT distribution of the ring current

Correspondence to:
S. Kumar,
sandeepk.iig@gmail.com

Citation:
Kumar, S., Veenadhari, B., Chakrabarty, D., Tulasi Ram, S., Kikuchi, T., & Miyoshi, Y. (2020). Effects of IMF By on ring current asymmetry under southward IMF Bz conditions observed at ground magnetic stations: Case studies. *Journal of Geophysical Research: Space Physics*, *125*, e2019JA027493. https://doi.org/10.1029/2019JA027493

Received 4 OCT 2019
Accepted 8 OCT 2020
Accepted article online 9 OCT 2020

Abstract In this paper, we have evaluated the role of interplanetary magnetic field (IMF) By on the asymmetry of the ring current during the main phase of geomagnetic storms. The mean *H* variations have been calculated using 31 ground magnetic stations over magnetic latitudes of 09–45° following the methodology of Li et al. (2011, https://doi.org/10.1029/2011JA016886). Further, the magnetic local time (MLT) variations in the *H* component at these stations w.r.t. the mean *H* were investigated for three cases of geomagnetic storms with varying southward IMF Bz and IMF By conditions. Significant ring current asymmetries were observed during the main phase of geomagnetic storms. The primary role of IMF Bz on the asymmetry of the ring current is observed from these cases. More importantly, the investigation brings out for the first time, the additional role of IMF By in influencing the MLT distribution of ring current observed at ground magnetic stations. Under southward IMF Bz conditions, it is shown based on SuperDARN and AMPERE data that IMF By can alter the MLT distribution of ring current under suitable conditions. The timescales of IMF By also play very important role in determining the asymmetry in the ring current. Under steady convection state, IMF By can rotate the convection cells based on its polarity, which in turn can change the MLT distribution of ring current observed by low-latitude ground stations. This investigation, thus, brings out the important role of IMF By on the asymmetric MLT distribution of ring current under southward IMF Bz.

1. Introduction

The interaction between solar wind and terrestrial magnetic fields is central to the studies of the effects of geomagnetic storms. During the southward interplanetary magnetic field (IMF) Bz condition in the solar wind, magnetic reconnection occurs between IMF Bz and the geomagnetic field which allows the transfer of energy from solar wind to the Earth's magnetosphere (Dungey, 1961; Gonzalez et al., 1994; Gonzalez & Tsurutani, 1987; Tsurutani et al., 1988). This reconnection is the primary cause of the geomagnetic storms. The global depression in *H* component of the geomagnetic field is observed on the ground during a geomagnetic storm. This *H* depression is mainly caused by the westward ring current encircling the Earth ~2 to 7 R_E and is formed by the energetic ions (~1 keV to approximately a few hundred keV) and electrons moving in opposite directions because of gradient and curvature drifts (Baumjohann & Treumann, 1996; Daglis et al., 1999; Hamilton et al., 1986). It is found that the ions with energies <50 keV contribute more significantly to the ring current than those with higher energies during the main phase of the storm and high energy protons dominate during the recovery phase and quiet times (Zhao et al., 2015).

The ring current is known to be asymmetric during the main phase of a geomagnetic storm and is characterized by dawn-dusk asymmetry with the dusk current being stronger than dawn current (Ebihara & Ejiri, 2000; Fok et al., 1996; Liemohn, Kozyra, Clauer, et al. 2001; Liemohn et al., 1999; Liemohn, Kozyra, Thomsen, et al., 2001). The dawn-dusk asymmetry in the ring current during disturbed time has been known for sometime (Sugiura & Chapman, 1960) and is generally attributed to be due to the generation of partial ring current (PRC) (Akasofu & Chapman, 1964; Cummings, 1966; Fukushima & Kamide, 1973; Kawasaki & Akasofu, 1971) during the main and early recovery phase of the storm. However, it was found that

most of the disturbance field part in PRC comes from the near-Earth field-aligned portion of the current loop (Crooker & Siscoe, 1981). Crooker and Siscoe (1981) further suggested that the cause of the asymmetry at low and middle latitude is the systematic twisting between Region-1 (R1) and Region-2 (R2) field-aligned currents (FACs). Global MHD simulations have shown that the dynamo of R1 FACs in the high-latitude boundary layer of outer magnetosphere is activated by high pressure plasma which is accumulated around the cusp and R1 dynamo moves hot plasma from plasma sheet to inner magnetosphere and this hot plasma assisted by gradient and curvature drifts causes PRC (R2 FAC dynamo) (Tanaka, 1995). Iijima and Potemra (1976) studied the average distribution of FACs and suggested the PRC closure through the R2 FACs. Thus, PRC is the primary cause of the dawn-dusk asymmetry in the ground H component and is associated with the closure through R2 FACs.

Tsuji et al. (2012) studied the local time (LT) distribution of ΔH during storm time and suggested that the dawn-dusk asymmetry of the ring current over low latitudes (10–35°) is due to the PRC, while over middle latitudes (35–55°) it is related to the DP2 fluctuations due to the convection electric field associated with R1 FACs on the dayside. It is found that during the main phase and early recovery phase most of the ring current is partial, closing through FACs into the polar ionosphere (Liemohn, Kozyra, Clauer, et al., 2001; Liemohn, Kozyra, Thomsen, et al., 2001). Li et al. (2011) through statistical study found that the PRC is located at dusk sector ~1800–2000 magnetic local time (MLT) and its contribution to ring current gradually decreases as the intensity of the storm increases. Shi et al. (2006) studied the effect of solar wind dynamic pressure enhancements on the asymmetric ring current and found that the pressure enhancement significantly increases the already existing strong asymmetry in the ring current during the main phase of the storm. Weygand and McPherron (2006) studied the dependence of ring current asymmetry on the storm phase by using Sym-H and Asym-H ratio and found that during the main phase, symmetric and asymmetric ring current grow together. Recently, Veenadhari et al. (2019) have shown that the PRC enhancement during southward IMF Bz with long duration (~8 hr) and attributed it to the storm time substorms.

Earlier studies have shown that the ring current is highly asymmetric during the main and early recovery phase and becomes symmetric during the recovery phase (DeForest & McIlwain, 1971). There are many current systems (e.g., Chapman-Ferraro current, symmetric ring current, PRC, tail current, and ionospheric currents) which contribute to the ground H component during the geomagnetic storm. These currents have different origin and effects at different MLTs. Several studies have addressed the question of the different sources affecting the symmetric H component during the main phase of the magnetic storm (Alexeev et al., 1996; Tsyganenko & Sitnov, 2005; Turner et al., 2000). Yu et al. (2010), using ground magnetic observations and global MHD simulations, showed that the variations in the northward component of geomagnetic field at low latitudes are mostly caused by magnetospheric currents, especially ring current. Several studies have examined the southward IMF Bz effects on ring current (Gonzalez et al., 1994; Kumar et al., 2015; Liemohn et al., 1999; Liemohn, Kozyra, Thomsen, et al., 2001; Lopez et al., 2009; Russell et al., 2001; Siscoe et al., 2004). Although there exists many studies that show the importance of IMF Bz (e.g., Liemohn et al., 1999; Liemohn, Kozyra, Thomsen, et al., 2001) and the solar wind dynamic pressure (e.g., Shi et al., 2006) on the asymmetry of the ring current, the role of IMF By on ring current asymmetry has not been explored enough. There are very few studies on the effects of IMF By on ring current (e.g., Mitchell et al., 2013). Mitchell et al. (2013) using simulation study suggested that the IMF By plays an important role in the ring current intensity as positive IMF By can increase the transpolar potential. However, they did not investigate the IMF By effects on ring current asymmetry. There are some studies which have shown that the changes in IMF By significantly modify the high- (Cumnock et al., 1992; Tulasi Ram et al., 2019) and low-latitude (Chakrabarty et al., 2017; Tulasi Ram et al., 2019) convection patterns under southward IMF Bz conditions. Heelis (1984) suggested that under southward IMF Bz condition the convection patterns get highly distorted depending upon the changes in magnitude and polarity of IMF By. Weimer (2001) has also shown that the FACs vary as the IMF clock angle changes and how FACs affect the associated electric potential pattern. It is shown that IMF By can introduce asymmetries in dayside convection and currents due to longitudinal stresses on reconnected magnetic field lines at the magnetopause (Greenwald et al., 1990; Saunders, 1989). Further, Saunders et al. (1992) have shown that the response of IMF By to IMF Bz associated with reconnection is seen within minutes near noon and later toward dawn and dusk. It was suggested that the high-latitude FACs can establish a strong polar-equatorial coupling during disturbed times, which makes

Table 1
List of Geomagnetic Observatories With Their IAGA Code and Geographic and Corrected Geomagnetic Latitude and Longitude Used for the Present Analysis

Station name	IAGA code	Geog. lat	Geog. long	CGM lat	CGM long
Alibag	ABG	18.64	72.87	12.08	145.46
Apia	API	−13.8	188.22	−15.6	262.65
Alice Springs	ASP	−23.76	133.88	−33.59	207.89
Beijing Ming Tombs	BMT	40.3	116.2	34.99	190.05
Stennis Space Centre	BSL	30.4	270.4	41.2	340.95
Chambon la Foret	CLF	48	2.3	43.33	79.19
Charters Towers	CTA	−20.1	146.3	−29.08	220.48
Fresno	FRN	37.1	240.3	42.98	303.97
Guimar-Tenerife	GUI	28.32	343.56	17.17	60.51
Hartebeesthoek	HBK	−25.88	27.70	−35.74	96.46
Hermanus	HER	−34.4	19.2	−42.33	82.9
Honolulu	HON	21.30	202	21.32	270.06
Jaipur	JAI	26.91	75.8	21.55	149.06
Kakioka	KAK	36.23	140.19	29.31	212.04
Kakadu	KDU	−12.6	132.5	−21.73	204.86
Kanoya	KNY	31.42	130.88	24.87	203.51
Kourou	KOU	5.21	307.27	9.46	23.62
Learmonth	LRM	−22.22	114.1	−32.46	186.53
Lanzhou	LZH	36.08	103.84	30.96	177.23
M'Bour	MBO	14.38	343.03	20.17	57.39
Memambetsu	MMB	43.9	144.2	37.12	215.74
Phuthuy	PHU	21.03	105.96	14.16	177.96
Pamatai	PPT	−17.6	210.4	−16.72	285.42
San Juan	SJG	18.11	293.85	27.46	10.73
San Pablo-Toledo	SPT	39.5	355.6	31.9	71.78
Tamanrasset	TAM	22.79	5.53	9.22	78.37
Tihany	THY	43.1	17.9	37.28	91.46
Trelew	TRW	−43.3	294.7	−29.94	4.92
Tsumeb	TSU	−19.2	17.58	−30.16	88.12
Tucson	TUC	32.2	249.2	39.76	314.86
Vassouras	VSS	−22.4	316.35	−19.63	23.7

the low-latitude fields fluctuate and sometimes can reverse their direction (Nopper & Carovillano, 1978). Some studies have demonstrated that the IMF By can influence the location of substorm onset and the morphology of associated nightside flows (Grocott et al., 2010; Milan et al., 2010). Further, Grocott and Milan (2014) extensively studied the IMF By influence on ionospheric convection and showed that for negative IMF By the electrodynamical divider of convection cells is approximately aligned with the noon-midnight meridian and for positive IMF By the divider is rotated clockwise. It has also been found that the time history of IMF plays an important role in governing the dynamics of the system specially in respect to the influence of IMF By, which is known to introduce dawn-dusk asymmetry in the magnetosphere-ionosphere system (Grocott et al., 2010; Milan et al., 2010; Murr & Hughes, 2007). It is also well known that IMF By component can significantly change the FACs distribution (Anderson et al., 2008; Carter et al., 2016; Tulasi Ram et al., 2019).

Earlier studies have shown IMF By effects on convection pattern using SuperDARN data (Grocott & Milan, 2014; Heelis, 1984; Ruohoniemi & Greenwald, 2005; Saunders et al., 1992) and FACs (Anderson et al., 2008; Carter et al., 2016; Nopper & Carovillano, 1978; Weimer, 2001). It is well established that ring current is asymmetric during the main phase of the magnetic storms (Ebihara & Ejiri, 2000; Fok et al., 1996; Liemohn, Kozyra, Clauer, et al. 2001; Liemohn et al., 1999; Liemohn, Kozyra, Thomsen, et al., 2001) due to the generation of PRC (Akasofu & Chapman, 1964; Cummings, 1966; Fukushima & Kamide, 1973; Kawasaki & Akasofu, 1971). PRC is the primary cause of the dawn-dusk asymmetry in the ground *H* component and is associated with the closure through R2 FACs (Iijima & Potemra, 1976). It has been found that IMF By component can significantly change the FACs distribution (Anderson et al., 2008; Carter et al., 2016; Tulasi Ram et al., 2019) and the high-latitude convection patterns (Grocott & Milan, 2014; Heelis, 1984; Ruohoniemi & Greenwald, 2005; Saunders et al., 1992). Thus, it is expected that IMF By can affect the MLT distribution of ring current asymmetry. However, it remained to be investigated how changes in IMF By during southward IMF Bz condition modify the ring current asymmetry. In this work, an attempt has been made to understand the effect of IMF By on MLT distribution of the ring current asymmetry. We have carefully picked few cases with different IMF By conditions under varying southward IMF Bz to investigate how ring current asymmetry behave under these conditions.

2. Data Set and Methodology

In order to study the evolution of ring current during the course of magnetic storms, the ground magnetic variations at low and middle latitudes are often used as a proxy. Ring current intensity and geomagnetic disturbances are described by hourly Dst index (Sugiura & Kamei, 1991) and 1-min resolution Sym-H index (Iyemori et al., 1992). It is to be noted here that for calculating Sym-H and Asym-H, only six ground magnetic stations, unevenly distributed in longitude and latitude, are used. Hence, these indices are not enough to capture the spatial/longitudinal asymmetry in the ring current. Therefore, to address the ring current asymmetry more accurately, 31 ground magnetic stations (http://www.intermagnet.org/data-donnee/download-eng.php) covering low to middle latitudes (09–45°) have been considered in the present analysis. Table 1 shows the list of all the stations used in the present analysis along with their geographic and corrected geomagnetic (CGM) coordinates. CGM coordinates have proven to be excellent tools in organizing geophysical phenomena controlled by the geomagnetic field. The ΔH of each station is calculated by subtracting 5 quiet days' average value as given in the below equation.

$$\Delta H = \frac{H - Hq}{\cos \varphi} \quad (1)$$

where H is a northward component and Hq is the average of 5 quietest days of that month (obtained from WDC Kyoto, http://wdc.kugi.kyoto-u.ac.jp/aeasy/index.html) at a particular station and φ is the magnetic latitude of that station.

Once ΔH is obtained from Equation 1, then the mean variation ΔH_m is calculated using a method described by Li et al. (2011). This method is different from the traditional Sym-H and Asym-H calculations (Iyemori et al., 1992), wherein cosine of the average latitude of all the stations is used.

$$\Delta H_m = \frac{1}{N} \sum_{n=1}^{N} \Delta H \quad (2)$$

where n is the variable that characterizes the number of stations and the N is the total number of stations (maximum value of n). Dipole-based approximation is invalid in defining MLT for the CGM coordinate system. Therefore, another approach in defining MLT for CGM coordinate system, provided by NASA Omniweb (https://omniweb.gsfc.nasa.gov/vitmo/cgm.html), is used. In this approach, it is assumed that at some UT instance, the local geographic meridian is at 0000 LT and the station is behind the geographic pole w.r.t. the Sun. If Earth rotates through an angle, in such a way that the station's local CGM meridian is moved to 0000 MLT, then the station is behind the CGM pole w.r.t. the Sun and this UT instance would be a local MLT midnight in UT. The solar wind interplanetary data like IMF Bz, IMF By, and solar wind dynamic pressure (Psw) were observed at 1 AU by combination of one or more spacecraft like Advanced Composition Explorer (ACE) or Wind and obtained from CDAWeb (https://cdaweb.sci.gsfc.nasa.gov/cgi-bin/eval1.cgi). The Sym-H (symmetric H index) and Auroral indices AU (eastward auroral electrojet) and AL (westward auroral electrojet) have been taken from WDC Kyoto (http://wdc.kugi.kyoto-u.ac.jp/aeasy/index.html). The solar wind interplanetary data and ground data like Sym-H, AU, and AL have 1-min temporal resolution. The convection map data from the Super Dual Auroral Radar Network (SuperDARN) of HF radars have been considered in this study to examine the high-latitude convection cells. Multiple HF radars provide coverage over larger area, and this large data set is used to generate global scale maps of ionospheric convection using a modified spherical harmonic fitting technique (Ruohoniemi & Baker, 1998; Shepherd & Ruohoniemi, 2000). SuperDARN data are obtained from the website (http://vt.superdarn.org/). Active Magnetosphere and Planetary Electrodynamics Response Experiment (AMPERE) uses continuous and global magnetic data from nearly polar orbiting satellites of Iridium constellation to derive the global distribution of FACs. The Iridium system of satellites (>70) has a polar orbit with an altitude of 780 km orbiting in six equally spaced orbital planes with at least 11 satellites in each plane. Each satellite carries an engineering magnetometer and measures the magnetic field perturbations. The radial currents into and away from the ionosphere are derived from the curl of spherical harmonic fit to the magnetic perturbations (Anderson et al., 2000, 2014). AMPERE data are obtained from the website http://ampere.jhuapl.edu/ and are used in the present study.

3. Results

We are presenting three cases of geomagnetic storm events with varying southward IMF Bz to investigate the IMF By effect on MLT distribution of ring current asymmetry as observed by ground magnetic stations. These three cases pertain to the main phase of moderate to intense geomagnetic storms.

Figure 1a shows the solar wind parameters in GSM coordinates along with AU, AL, and Sym-H indices during the magnetic storm of 1 June 2013. The variation of IMF Bz, IMF By, solar wind dynamic pressure (Psw), AU, AL, and Sym-H is shown in Figure 1a from top to bottom, respectively. The 1 June 2013 storm is an example of intense geomagnetic storm with Sym-H < -100 nT. IMF Bz was long and steadily southward for the investigated interval (0200–0700 UT) with magnitude ~−20 nT. IMF By was positive for most of the interval except during 0310–0330 UT and close to 0630 UT, when it turned negative for short durations. IMF By was strongly positive with magnitude of ~15 nT at ~0400 UT. Solar wind dynamic pressure (Psw) had a small enhancement around 0330 UT, when Psw gradually reached close to ~6 nPa and was constant at ~3–4 nPa for the rest of the interval. AU and AL indices showed fluctuations after 0215 UT. AL index

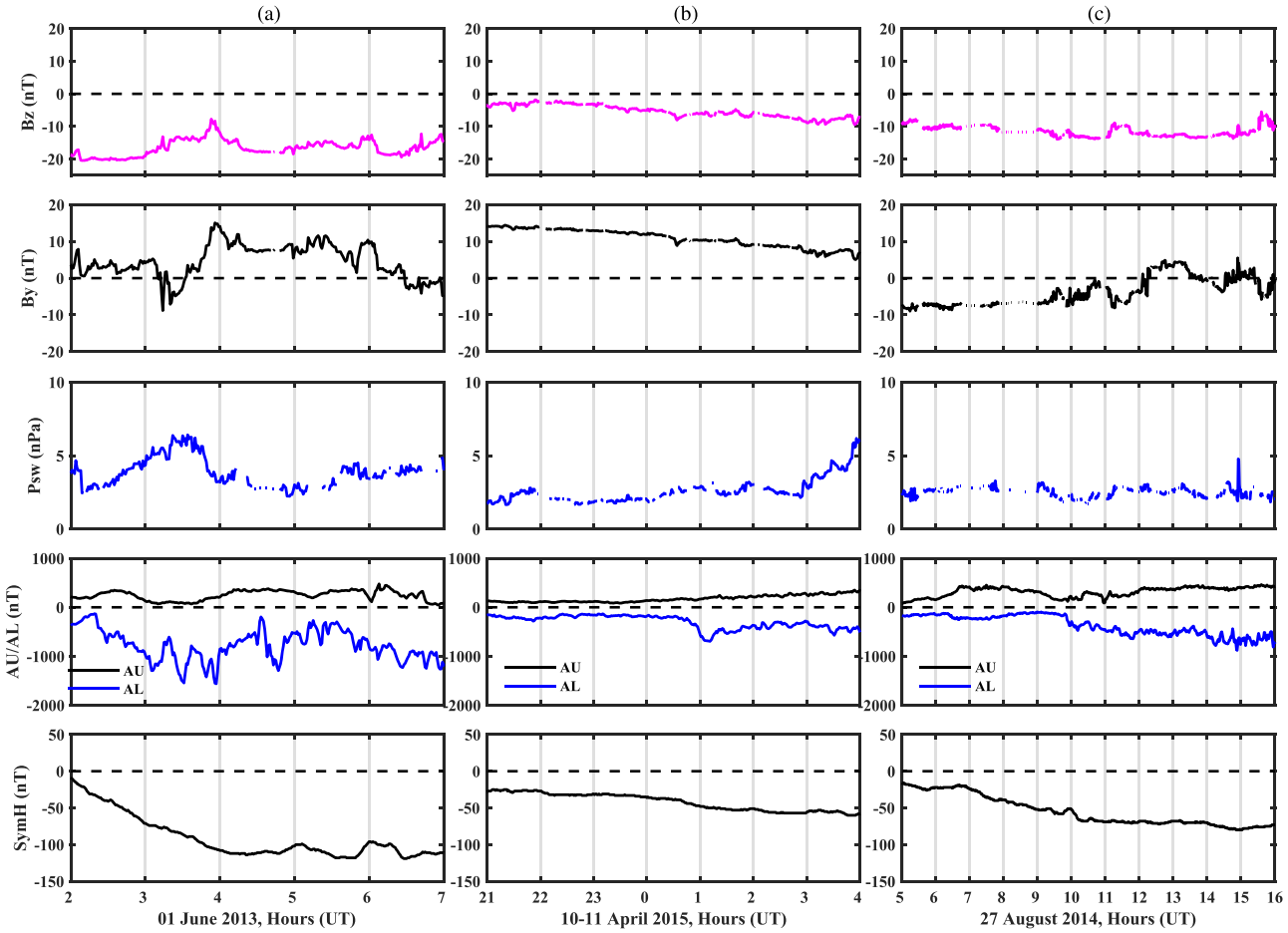

Figure 1. Variation in the interplanetary parameters and geomagnetic indices for geomagnetic storms on (a) 1 June 2013, (b) 10–11 April 2015, and (c) 22 January 2012. Each panel from top to bottom shows IMF Bz (in nT), IMF By (in nT), solar wind dynamic pressure, Psw, (in nPa), auroral indices AU and AL (in nT), and Sym-H (in nT).

showed intensification after 0230 to 0400 UT; there was again strong depression in AL around 0430 UT suggesting strong substorm activity. The variation in Sym-H in Figure 1a shows development of the main phase in response to the southward IMF Bz condition.

Figure 1b shows another example of long southward IMF Bz phase of geomagnetic storm on 10–11 April 2015. Figure 1b from top to bottom shows the variation of IMF Bz, IMF By, Psw, AU, AL, and Sym-H. IMF Bz was southward throughout the interval under consideration with magnitude of ~−10 nT. The IMF By was positive, and its magnitude was decreasing with the time. However, its polarity did not change during this interval. The Psw was almost constant from 2100 UT on 10 April 2015 to 0300 UT on 11 April 2015. It increased from 0300 UT onward on 11 April 2015. Auroral indices did not show any significant variations until 0100 UT on 11 April 2015. There was a weak and ephemeral intensification in AL around 0100 UT on 11 April 2015. However, this can hardly be qualified as due to the significant substorm activity considering the minimum magnitude of AL. Sym-H index can also be seen decreasing during the considered interval in response to the IMF Bz. This is an example of moderate geomagnetic storm with Sym-H ~ −50 nT.

Figure 1c from top to bottom shows the IMF Bz, IMF By, Psw, AU, AL, and Sym-H variation for the 27 August 2014 magnetic storm. IMF Bz was southward with magnitude around −10 nT throughout the considered interval. IMF By was negative initially from 0500 to 1200 UT. It changed polarity from 1200 to 1330 UT with small positive value of ~5 nT. Psw was constant throughout the interval except 1500 UT, with a small peak (~5 nPa). There was not much variation in AU and AL indices initially from 0500 to 1000 UT. However, after 1000 UT, AL and AU index shows gradual intensification suggesting a period of enhanced steady convection. The minimum value of Sym-H was ~−80 nT.

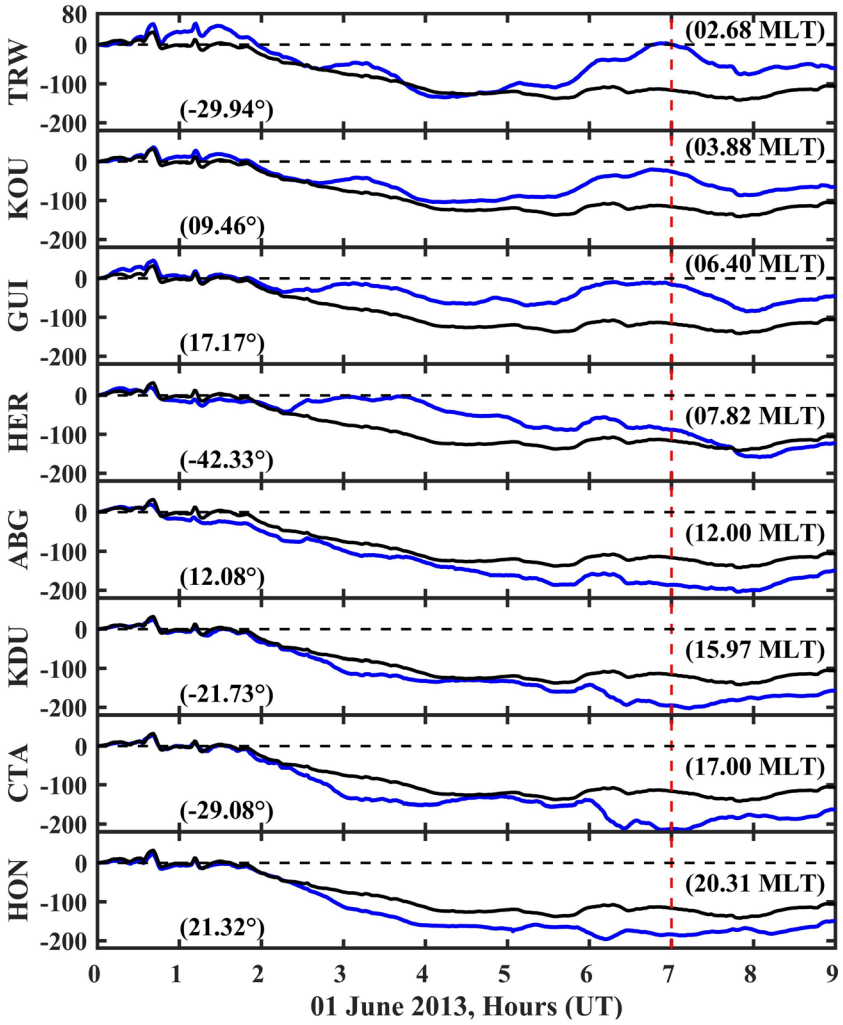

Figure 2. The variations of ΔH component with mean ΔH_m over different MLT sector for 1 June 2013. The black line is the mean ΔH_m component over all stations, and the blue line shows the ΔH variation at the individual station. The time written in brackets shows the MLT of each individual station corresponding to 0700 UT, and number written in each panel represents the CGM latitude of that particular station.

Figure 2 shows ΔH variations along with ΔH_m of some selected individual stations at different MLTs during the magnetic storm of 1 June 2013. For the sake of brevity, only one typical example of 1 June 2013 is shown here. The blue curve shows the ΔH of the corresponding station, and black curve is the mean variation ΔH_m of all the stations listed in Table 1. The time written in brackets at each panel shows the corresponding MLT of that particular station at 0700 UT (marked with vertical red line), and number written in degrees is the CGM latitude of that station. The main phase started around 0200 UT. It can be seen in Figure 2 that at the peak of the storm ~0700 UT there is a clear dawn-dusk asymmetry as the stations located at dawn sector (0300–0700 MLT) (TRW, KOU, GUI, and HER) show positive ΔH deviations with respect to ΔH_m. On the other hand, the stations located at dusk sector (1700–2100 MLT) (CTA and HON) show negative ΔH deviations with respect to ΔH_m. All the stations are showing positive/negative ΔH deviations w.r.t. ΔH_m at dawn/dusk side throughout the main phase, which is a typical feature of ring current asymmetry. In order to see the effect of storm intensity on ring current asymmetry, we compared the maximum and minimum values of $\Delta H_{\text{asy}} = \Delta H - \Delta H_m$ for the minimum value of Sym-H during the time interval shown in Figure 1. This ΔH_{asy} is the difference between the H component (blue curve of Figure 2) of the individual station and the ΔH_m (black curve of Figure 2). For event 1 June 2013 ($\text{SymH}_{\text{min}} = -119$ nT at 0630 UT), ΔH_{asy} max = 98 nT

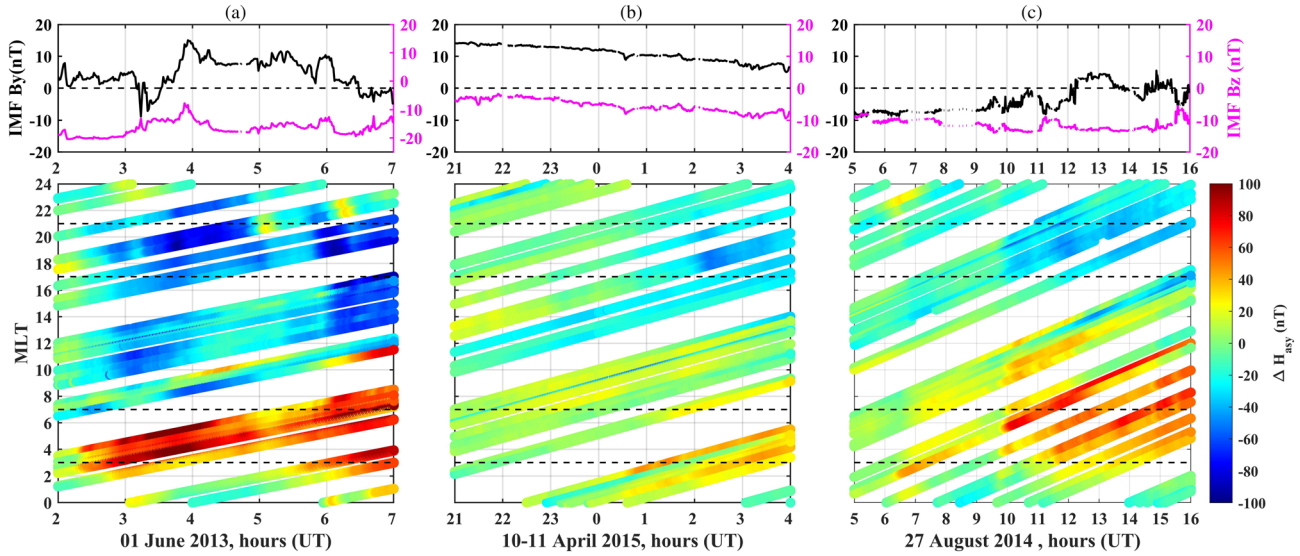

Figure 3. The top panel shows the variation of IMF Bz and By, and the bottom panel shows the variation of ΔH_{asy} with MLT and onset time (UT) during the main phase of the magnetic storms (a) 1 June 2013, (b) 10–11 April 2015, and (c) 27 August 2014. Time resolution is 1 min. Color bar shows the strength of ΔH_{asy}. Horizontal dashed lines represent 0300–0700 MLT and 1700–2100 MLT.

and ΔH_{asy} min = −73 nT. Similarly, for 11 April 2015 ($SymH_{min}$ = −60 nT at 0350 UT), ΔH_{asy} max = 48 nT and ΔH_{asy} min = −34 nT, and for 27 August 2014 ($SymH_{min}$ = −80 nT at 1500 UT), ΔH_{asy} max = 67 nT and ΔH_{asy} min = −40 nT. It can be seen that the intensity of ring current asymmetry depends on the intensity of storm (IMF Bz). The other two storms also show the same features of ring current asymmetry as Figure 2 but with less intensity.

Figure 3a shows the IMF Bz (pink color) and IMF By (black color) in the top panel for 1 June 2013. These are reproduced in all panels (a–c, all the three events) of Figure 3 for ready reference. The bottom panel shows the deviations of ΔH_{asy} with 1-min resolution for the magnetic storm of 1 June 2013 during the main phase with corresponding MLT (*Y* axis) and UT (*X* axis). The horizontal dashed lines represent the dawn (0300–0700 MLT) and dusk sector (1700–2100). The color code shows the magnitude of ΔH_{asy} deviation. It can be seen from the bottom panel of Figure 3a that there is a clear asymmetry in the ring current. During 0230 UT, the ΔH_{asy} deviations in dawn sectors are strongly positive, and at the same time, the afternoon and dusk sectors show negative deviations. IMF By was strongly positive during 0400–0600 UT. Around 0500 UT, it can be seen that MLT sector of 2100–2400 has some positive ΔH_{asy} deviations contrary to the expected negative deviations as per dawn-dusk asymmetry.

Figure 3b top panel shows the IMF Bz and IMF By, and the bottom panel shows the ΔH_{asy} deviations with UT and MLT for 10–11 April 2015. It can be seen from Figure 3b that there is asymmetry in the ring current. However, it does not appear as strong as observed in 1 June 2013. The reason is that it has less magnitude of IMF Bz compared to 1 June 2013 magnetic storm and both are shown in same color scale for the sake of comparison. IMF By was positive throughout the considered interval. It can be seen around 2200 UT, the dawn sector has positive ΔH_{asy} deviations (shown by green and yellow color). However, after 2300 UT the positive ΔH_{asy} deviations can be seen moving toward afternoon sector and negative ΔH_{asy} deviations can be seen moving from afternoon to dusk sectors. A clear and strong ring current asymmetry can be seen after 0100 UT, when dawn sector shows strong positive ΔH_{asy} deviations (red color) and afternoon to dusk sector shows negative deviations (cyan color).

Figure 3c top and bottom panel shows the IMF Bz, IMF By, and ΔH_{asy} deviations with UT and MLT for 27 August 2014 geomagnetic storm, respectively. It can be seen from Figure 3c there is a strong ring current asymmetry after 0600 UT. IMF By was negative till 1200 UT. Interestingly, after IMF By turned positive, the positive ΔH_{asy} deviations shifted from dawn to afternoon sector.

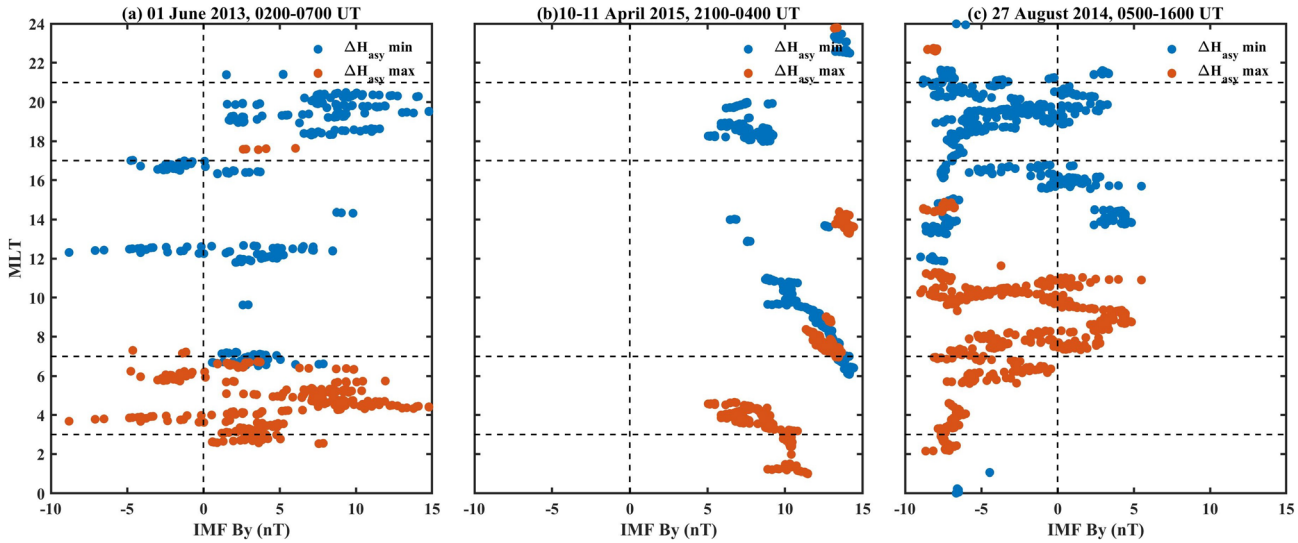

Figure 4. Variation of MLT location of maximum and minimum values of ΔH_{asy} deviation shown by red and blue color, respectively, with IMF By for (a) 1 June 2013, (b) 10–11 April 2015, and (c) 27 August 2014. Time interval shown is same as Figure 1.

4. Discussion

In order to examine the IMF By role on ring current asymmetry, three cases of geomagnetic storms with steady southward IMF Bz are investigated in this work. Although indications of the possible IMF By effects on the ring current asymmetry are captured by Figure 3 and the maximum/minimum ΔH_{asy} deviations are seen to deviate from the expected dawn and dusk sectors in varying degrees when IMF By is positive under southward IMF Bz conditions, further attempts are made to confirm this. The results from these efforts will be discussed in the ensuing section.

Figure 4 brings out the role of IMF By on ring current asymmetry. In this figure, the MLT location of maximum and minimum ΔH_{asy} values is plotted with IMF By. Figure 4 shows the MLT location of maximum (red color) and minimum (blue color) ΔH_{asy} values with IMF By for (a) 1 June 2013, (b) 10–11 April 2015, and (c) 27 August 2014. Each point in Figure 4 corresponds to 1-min sampling data. It can be seen from Figure 4a that minimum ΔH_{asy} deviations are mostly in the afternoon sector and maximum ΔH_{asy} deviations are in dawn sector. It is interesting to note that during positive IMF By some peak ΔH_{asy} values can be seen in dusk sector. These are the points when asymmetry was weak and started developing (around 0200 UT, Figure 3a). The polarity of IMF By was mostly positive during the considered interval (Figure 1a). It was negative for very short interval, and therefore, fewer number of data points are there corresponding to negative IMF By. It is also to be noted that IMF Bz was very strong (~−20 nT) during this interval. It has been suggested that for strong southward IMF Bz, the magnetosphere is quickly able to reach an equilibrium state such that the other solar wind parameters have very little effect on the system under these circumstances (Grocott & Milan, 2014). It can be seen from Figure 4a that the usual dawn-dusk asymmetry is observed very clearly due to very strong convection. Figure 4b shows the variation of MLT location of maximum and minimum ΔH_{asy} deviation with IMF By for 11 April 2015. In this case the IMF By was positive throughout the considered interval (Figure 1b). It can be seen from Figure 4b that with increasing magnitude of positive IMF By, the maximum ΔH_{asy} deviations shift from the dawn sector to the afternoon sector and the minimum ΔH_{asy} deviations shift from the dusk sector to the afternoon sector. IMF Bz in this case was negative (<−9 nT) throughout the interval. However, it is to be noted that IMF By was positive for ~20 hr (not shown here). It has been shown that the history of IMF with timescales anywhere up to 12 hr is expected to play a very important role in governing the dynamics of the magnetosphere ionosphere system particularly in respect to the influence of IMF By (Grocott & Milan, 2014; Grocott et al., 2007; Milan et al., 2006). In 10–11 April 2015 storm, IMF By had significant timescale to alter the magnetosphere ionosphere system. Figure 4c shows the variation of MLT location of maximum and minimum ΔH_{asy} deviation with IMF By for 27 August 2014. In this case, polarity of IMF By was negative mostly with some positive variation for couple of hours (Figure 1c).

IMF Bz was southward with values ~−12 nT throughout the considered interval. It can be seen from Figure 4c that for large negative IMF By the maximum ΔH_{asy} deviations are scattered across the dawn-morning sector and the minimum ΔH_{asy} deviations are scattered across the dusk sectors. During this interval the ring current asymmetry was developing (Figure 3c). However, for positive IMF By values, maximum ΔH deviations are located at prenoon sector and minimum ΔH_{asy} deviations are located in the dusk sector as now the asymmetry was well developed (Figure 3c). In this case IMF By was positive for very short interval of time. Therefore, it is clear from Figure 4b that under southward IMF Bz, positive IMF By with suitable timescales (~12 hr) has discernible effect in shifting the MLT of the ring current asymmetry.

In order to support the IMF By effects on ring current asymmetry, high-latitude convection patterns, obtained from SuperDARN of HF radars, are investigated. Further, to examine the possible changes in the high-latitude FACs, the derived radial currents from the AMPERE have been considered. Figures 5–7 capture a few important features of these observations carefully selected to show different variations and combinations of IMF By. It will not be convenient to show the convection maps for the entire interval.

Figure 5 shows the convection maps obtained from SuperDARN network (a–c) and radial current density obtained from AMPERE (d–f) for 1 June 2013. Figure 5a shows convection map for 0300–0302 UT. During this interval, IMF By was positive. The sizes of the dawn (red) and dusk cells (blue) were comparable at this time. Figure 5d shows the radial current density derived from the AMPERE measurements. Red and blue color shows the upward (away) and downward (into) currents, respectively. Thus, the currents at high latitude (inner circle) represent the R1, and the lower latitude (outer) represents the R2 FACs. It can be seen that the FACs are stronger in afternoon and prenoon sector. Figure 5b shows the convection maps for 0314–0316 UT. IMF By was negative during this time interval. The size of the dawn cell appears to get slightly bigger at this time due to the increased convection. The electrodynamical divider between these cells is roughly aligned to noon-midnight meridian. FACs distribution can also be seen changed as dusk and dawn sector current becomes stronger. Figure 5c shows the convection maps for 0416–0418 UT. IMF By was positive during this interval. The dusk cell at this time almost engulfed the dawn cell that shrunk significantly in size. Dusk cell size has increased significantly. Therefore, there is significant change in size of the convection cells as IMF Bz was strong southward. Figure 5c shows the dusk cell expansion toward noon to prenoon sector. At the same time, from Figure 5f it can be seen that FACs distribution has also changed significantly as now stronger currents can be seen in noon sector compared to previous (Figure 5e) distribution. The currents are enhanced in dawn, afternoon, and dusk sectors.

Figure 6a shows the convection maps for the time interval 2200–2202 UT for 10 April 2015. IMF By was positive during this interval. The magnitude of IMF Bz was small; thus, convection cells are not as strong as in the case of 1 June 2013. Nevertheless, the dusk cell is much bigger than the dawn cell similar to Figure 5c. In addition, the electrodynamic boundary between the dawn and dusk cells is not aligned with the noon-midnight boundary and seems to have undergone a clockwise rotation similar to Figure 5c. At the same time, the FACs distribution (Figure 6d) shows asymmetry as the dawnside FACs are much stronger than the dusk ones. Figure 6b shows the convection maps for the time interval of 2340–2342 UT. IMF By was positive, and the magnitude of southward IMF Bz also increased during this interval. It can be observed that convection cells have gotten bigger and undergone further clockwise rotation. From Figure 6e it can be seen that FACs in the afternoon-midnight sector are weakened significantly. Figure 6c shows the convection cells for 0102–0104 UT for the 11 April 2015. Southward IMF Bz was strong during this interval, and IMF By was positive. It can be seen from Figure 6c the convection cells are now even stronger and bigger in size with clockwise extension in MLT region at higher latitudes. The relative changes in the size of the dawn and dusk cells might have been due to the changes in the relative magnitudes of IMF Bz and IMF By (Heelis, 1984; Ruohoniemi & Greenwald, 2005; Tanaka, 2007). Figure 6f shows there is significant modification in FACs distribution during this interval. The region of stronger FACs seems to have rotated clockwise, and at this point of time, dawn to midnight sector currents are stronger than other sectors. It can also be seen from Figures 6a and 6b the electrodynamical divider between these cells underwent a clockwise rotation from the original noon-midnight line which is consistent with earlier observed positive IMF By effect (e.g., Chakrabarty et al., 2017; Heelis, 1984; Ruohoniemi & Greenwald, 2005; Tanaka, 2007).

Figure 7a shows the convection cells of 1102–1104 UT for 27 August 2014. IMF By was negative during this interval. It can be seen that the dusk cell is stronger than dawn cell. The electrodynamic divider between

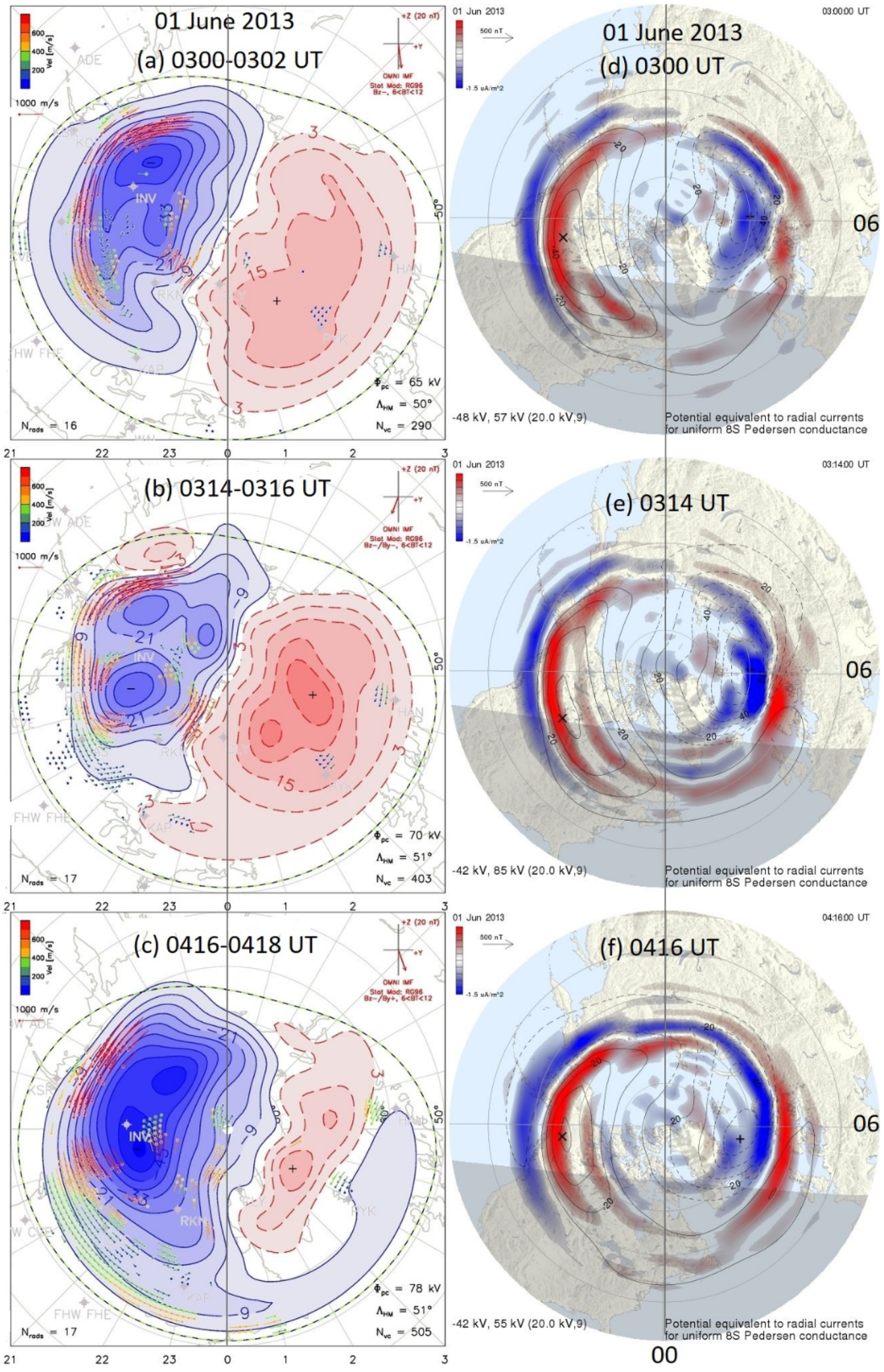

Figure 5. SuperDARN ionospheric convection maps along with DP2 contours during (a) 0300–0302 UT, (b) 0314–0316 UT, and (c) 0416–0418 UT on 1 June 2013. AMPERE-derived radial current densities during (d) 0300 UT, (e) 0316 UT, and (f) 0416 UT on 1 June 2013. Here red and blue color shows the upward (away) and downward (into) currents, respectively.

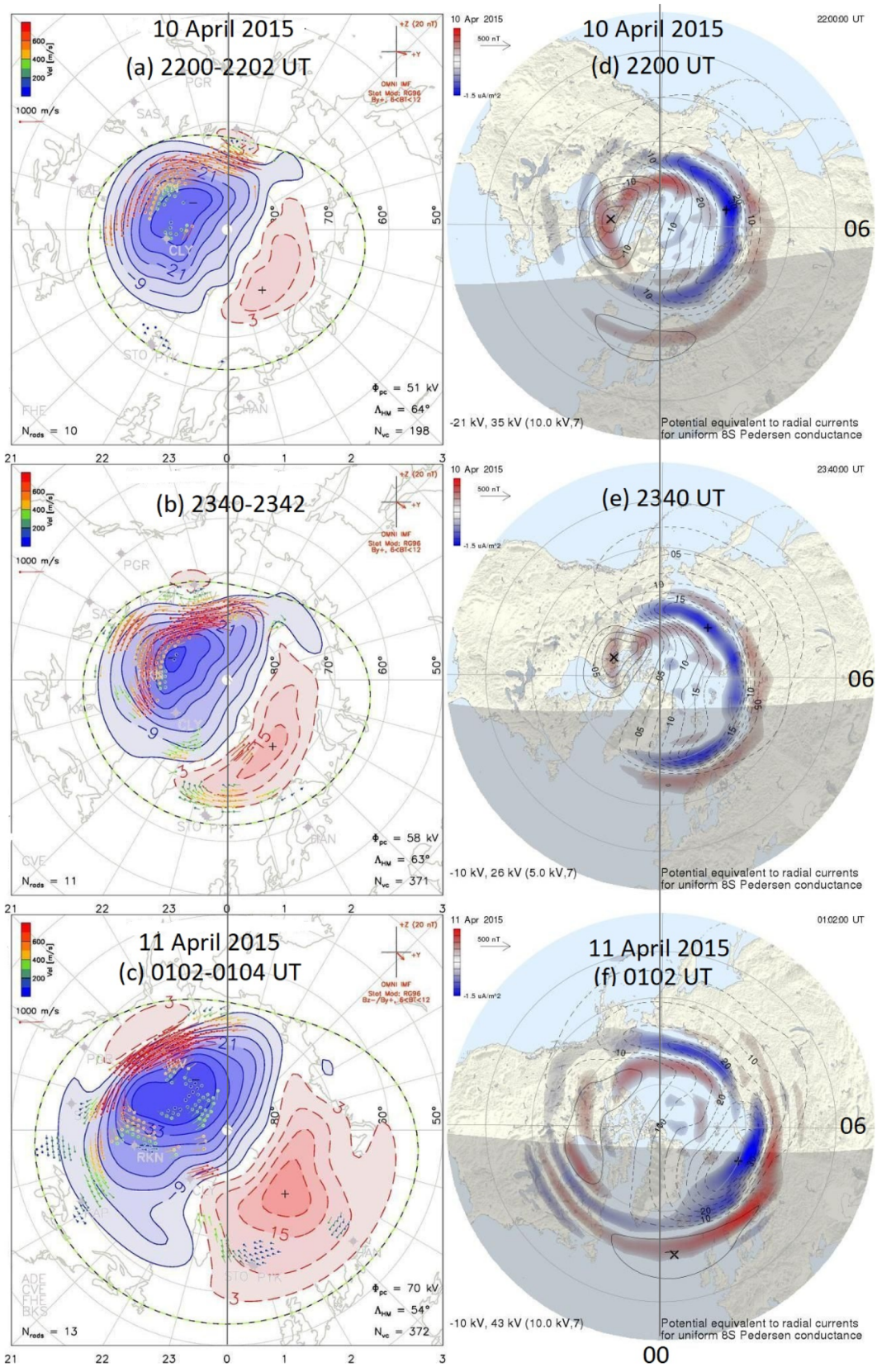

Figure 6. Same as Figure 5 except the date and time interval. SuperDARN plots during (a) 2200–2202 UT, (b) 2340–2342 UT, and (c) 0102–0104 UT on 10–11 April 2015. AMPERE-derived radial current densities during (d) 2200 UT, (e) 2340 UT, and (f) 0102 UT on 10–11 April 2015.

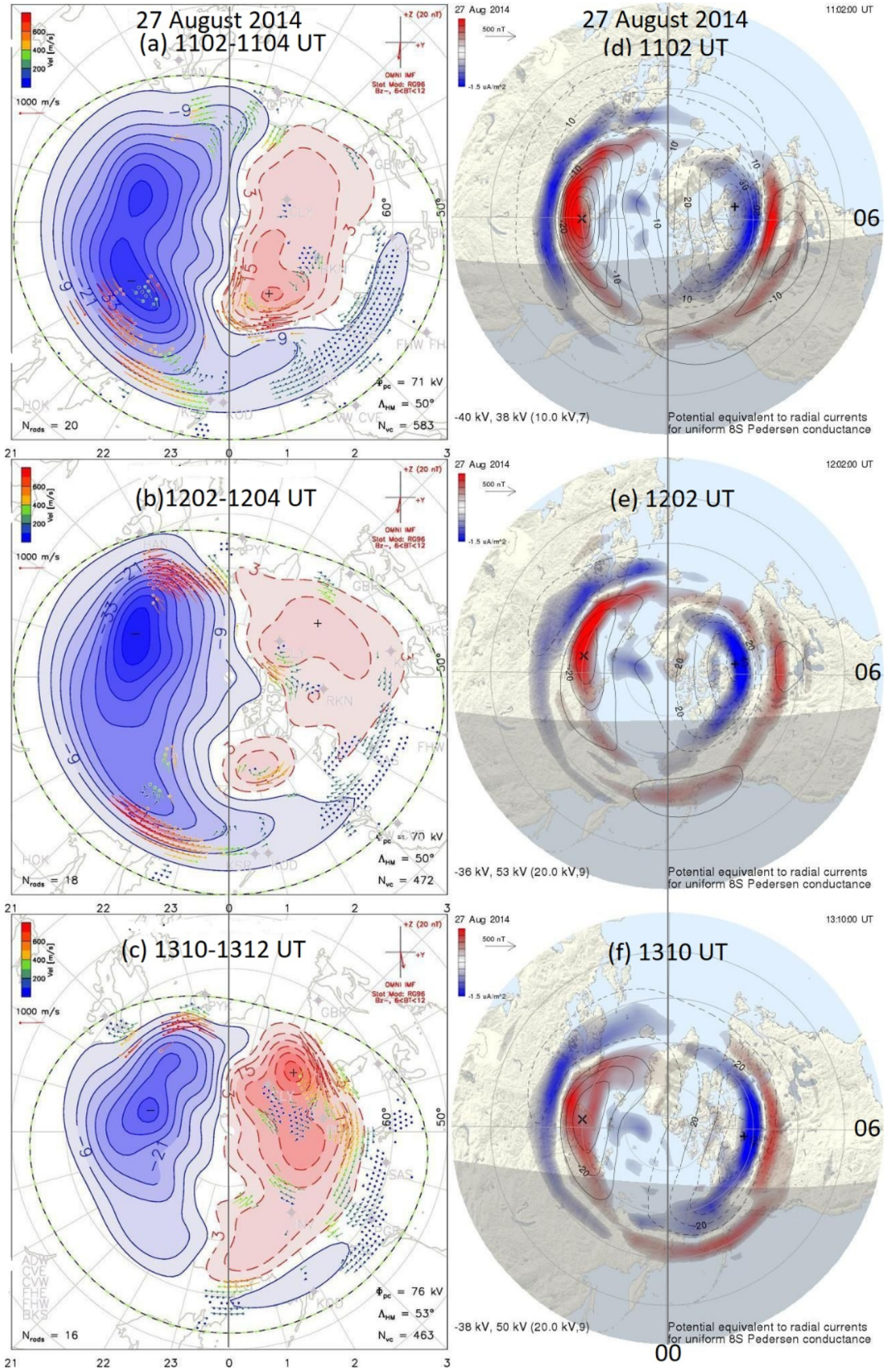

Figure 7. Same as Figure 5 except the date and time interval. SuperDARN plots during (a) 1102–1104 UT, (b) 1202–1204 UT, and (c) 1310–1312 UT on 27 August 2014. AMPERE-derived radial current densities during (d) 1102 UT, (e) 1202 UT, and (f) 1310 UT on 10–11 April 2015.

the dawn and dusk cells seems to be grossly aligned with the noon-midnight line. Figure 7d shows the FACs distribution for the same interval, and it can be seen that the currents are stronger in the afternoon and dusk sectors. Figure 7b shows the convection map for 1202–1204 UT. The IMF By was negative during this interval, and electrodynamical divider between these cells can be seen approximately aligned with noon-midnight meridian. The similar rotation in FACs can be seen from Figure 7e as now currents are stronger in dawn and afternoon sectors compared to other sectors. Figure 7c shows the convection cells for the 1310–1312 UT. IMF By was positive during this interval. The IMF By was positive for very short interval ~1 hr. Therefore, no significant rotation of convection cells was observed from Figure 7c. Although the relative size of dawn cell has increased whereas size of dusk cells has decreased compared to Figure 7b. It can also be seen from Figure 7f that FACs distribution has also been changed in accordance with convection cells.

Although the potential contours in the SuperDARN convection maps are synthetically generated and superimposed and depends upon the number of velocity vectors observed (Cousins & Shepherd, 2010; Ruohoniemi & Baker, 1998; Ruohoniemi & Greenwald, 2005; Shepherd & Ruohoniemi, 2000), the maps do provide an idea about the relative size and orientation of the dawn and dusk cells in response to changes in solar wind parameters like IMF Bz and By. It should be noted that the velocity vectors from SuperDARN HF radar observations are very less in some cases shown here. Hence, the constructed maps are based on convection model. These maps may have some uncertainty in the size and shape of the convection cells. However, in the present study, we are interested in the rotation of the convection cells, and these maps do provide an idea about the relative rotation of these convection cells. Grocott and Milan (2014) have extensively studied the role of IMF clock angle and the IMF timescale on the ionospheric convection. They found that the nature of ionospheric convection changes with the IMF clock angle and if the timescale, that is, the length of time that a similar clock angle has been maintained, increases, then the observed convection patterns evolve away significantly from the averaged patterns. As the rotation of the dawn and dusk cells as well as the FACs corresponding to the changes in IMF By for the three events under consideration is consistent with the existing understanding (Anderson et al., 2005, 2008; Carter et al., 2016; Grocott & Milan, 2014; Heelis, 1984; Ruohoniemi & Greenwald, 2005; Tanaka, 2007), the important role of positive IMF By during these events is strengthened further. Therefore, deviations from the dawn-dusk asymmetry as revealed by Figures 3 and 4 corresponding to positive IMF By provide credence to the important role played by IMF By in modifying the ring current asymmetry. The storm time convection strengthens the ring current during the main phase of the storm (Gonzalez et al., 1994; Miyoshi & Kataoka, 2005; Tsurutani et al., 1988), and ring current is asymmetric due to the generation of storm time PRC (Fukushima & Kamide, 1973; Kawasaki & Akasofu, 1971), and a dawn-dusk asymmetry is observed (Liemohn, Kozyra, Clauer, et al. 2001; Liemohn et al., 1999; Liemohn, Kozyra, Thomsen, et al., 2001). PRC is associated directly to R2 FACs through its closure in ionosphere (Brandt et al., 2008; Iijima & Potemra, 1976). Further, changes in IMF By under southward IMF Bz can significantly change the MLT distribution of the dawn-dusk convection cells (Heelis, 1984; Tanaka, 2007) and FACs (Anderson et al., 2005, 2008; Carter et al., 2016) which in turn changes the MLT distribution of ring current asymmetry observed at ground magnetic stations under suitable conditions.

5. Summary

In this work, we investigated three cases of varying southward IMF Bz geomagnetic storms using 31 ground magnetic stations (09–45° MLat) to identify the IMF By effects on ring current asymmetry. It is found that under southward IMF Bz, a clear asymmetry persists in the ring current throughout the main phase. The intensity and the duration of southward IMF Bz play a very important role in the ring current. Under strong convection (high magnitude of southward Bz) the effect of other parameters is not clearly observed. IMF By with longer timescale (~12 hr or more) has shown to change the MLT distribution of the ring current observed at ground. Positive (negative) IMF By can rotate the electrodynamical boundary between the dawn and dusk convection cells clockwise (counter clockwise). IMF By also changes the MLT distribution of associated FACs. Thus, the maximum and minimum ΔH_{asy} deviations (Figure 4) change MLT distribution as per the convection cell rotation and FACs distribution. This in turn alter the MLT distribution of ring current asymmetry. Therefore, the effects of IMF By and its timescales on the ring current asymmetry need to be studied in more detail using observation and simulations.

Acknowledgments

The authors acknowledge the Coordinated Data Analysis Web (CDAWeb) (https://cdaweb.sci.gsfc.nasa.gov/index.html/) and Kyoto World Data Center for Geomagnetism (http://wdc.kugi.kyoto-u.ac.jp/wdc/Sec3.html) for providing solar wind interplanetary and Sym-H data, respectively. The results presented in this paper rely on data collected at magnetic observatories. We thank the national institutes that support them and INTERMAGNET for promoting high standards of magnetic observatory practice (www.intermagnet.org). The authors acknowledge the use of SuperDARN data. SuperDARN is a collection of radars funded by national scientific funding agencies of Australia, Canada, China, France, Japan, South Africa, the United Kingdom, and the United States, and the data are available from the Virginia Tech SuperDARN website (http://vt.superdarn.org/). We also thank the AMPERE team and the AMPERE Science Center (http://ampere.jhuapl.edu/) for providing the Iridium-derived data products. S. K. and Y. M. works are supported by PWING project. The PWING project is funded as the Grant-in-Aid for Specially Promoted Research (16H06286) by the Japan Society for the Promotion of Science (JSPS) and the Ministry of Education, Culture, Sports, Science and Technology (MEXT). Y. M. is also supported by Grant-in-Aid for Research (15H05815, 15H05747, and 20H01959).

References

Akasofu, S.-I., & Chapman, S. (1964). On the asymmetric development of magnetic storm fields in low and middle latitudes. *Planetary and Space Science*, *12*(6), 607–626. https://doi.org/10.1016/0032-0633(64)90008-X

Alexeev, I. I., Belenkaya, E. S., Kalegaev, V. V., Feldstein, Y. I., & Grafe, A. (1996). Magnetic storms and magnetotail currents. *Journal of Geophysical Research*, *101*(A4), 7737–7747. https://doi.org/10.1029/95JA03509

Anderson, B. J., Korth, H., Waters, C. L., Green, D. L., Merkin, V. G., Barnes, R. J., & Dyrud, L. P. (2014). Development of large-scale Birkeland currents determined from the Active Magnetosphere and Planetary Electrodynamics Response Experiment. *Geophysical Research Letters*, *41*, 3017–3025. https://doi.org/10.1002/2014GL059941

Anderson, B. J., Korth, H., Waters, C. L., Green, D. L., & Stauning, P. (2008). Statistical Birkeland current distributions from magnetic field observations by the Iridium constellation. *Annales de Geophysique*, *26*, 671–687. https://doi.org/10.5194/angeo-26-671-2008

Anderson, B. J., Ohtani, S.-I., Korth, H., & Ukhorskiy, A. (2005). Storm time dawn-dusk asymmetry of the large-scale Birkeland currents. *Journal of Geophysical Research*, *110*, A12220. https://doi.org/10.1029/2005JA011246

Anderson, B. J., Takahashi, K., & Toth, B. A. (2000). Sensing global Birkeland currents with Iridium engineering magnetometer data. *Geophysical Research Letters*, *27*(24), 4045–4048. https://doi.org/10.1029/2000GL000094

Baumjohann, W., & Treumann, R. A. (1996). *Basic space plasma physics*. London: Imperial Coll Press. https://doi.org/10.1142/p015

Brandt, P. C., Zheng, Y., Stirelis, T. S., Oksavik, K., & Rich, F. J. (2008). The linkage between the ring current and the ionosphere system. In P. M. Kintener, A. J. Coster, T. Fuller-Rowell, et al. (Eds.), *Midlatitude ionospheric dynamics and disturbances*, *Geophysical monograph series* (Vol. 181, pp. 135–143). Washington DC: AGU.

Carter, J. A., Milan, S. E., Coxon, J. C., Walach, M.-T., & Anderson, B. J. (2016). Average field-aligned current configuration parameterized by solar wind conditions. *Journal of Geophysical Research: Space Physics*, *121*, 1294–1307. https://doi.org/10.1002/2015JA021567

Chakrabarty, D., Hui, D., Rout, D., Sekar, R., Bhattacharyya, A., Reeves, G. D., & Ruohoniemi, J. M. (2017). Role of IMF By in the prompt electric field disturbances over equatorial ionosphere during a space weather event. *Journal of Geophysical Research: Space Physics*, *122*, 2574–2588. https://doi.org/10.1002/2016JA022781

Cousins, E. D. P., & Shepherd, S. G. (2010). A dynamical model of high-latitude convection derived from SuperDARN plasma grift measurements. *Journal of Geophysical Research*, *115*, A12328. https://doi.org/10.1029/2010JA016017

Crooker, N. U., & Siscoe, G. L. (1981). Birkeland currents as the cause of the low-latitude asymmetric disturbance field. *Journal of Geophysical Research*, *86*(A13), 11,201–11,210. https://doi.org/10.1029/JA086iA13p11201

Cummings, W. D. (1966). Asymmetric ring currents and the low-latitude disturbance daily variation. *Journal of Geophysical Research*, *71*(19), 4495–4503. https://doi.org/10.1029/JZ071i019p04495

Cumnock, J. A., Heelis, R. A., & Hairston, M. R. (1992). Response of the ionospheric convection pattern to a rotation of the interplanetary magnetic field on January 14, 1988. *Journal of Geophysical Research*, *97*(A12), 19,449–19,460. https://doi.org/10.1029/92JA01731

Daglis, I. A., Thorne, R. M., Baumjohann, W., & Orsini, S. (1999). The terrestrial ring current: Origin, formation, and decay. *Reviews of Geophysics*, *37*(4), 407–438. https://doi.org/10.1029/1999RG900009

DeForest, S., & McIlwain, C. E. (1971). Plasma clouds in the magnetosphere. *Journal of Geophysical Research*, *76*(16), 3587–3611. https://doi.org/10.1029/JA076i016p03587

Dungey, J. W. (1961). Interplanetary magnetic field and the auroral zones. *Physical Review Letters*, *6*(2), 47–48. https://doi.org/10.1103/PhysRevLett.6.47

Ebihara, Y., & Ejiri, M. (2000). Simulation study on fundamental properties of the storm-time ring current. *Journal of Geophysical Research*, *105*(A7), 15,843–15,859.

Fok, M. C., Moore, T. E., & Greenspan, M. E. (1996). Ring current development during storm main phase. *Journal of Geophysical Research*, *101*(A7), 15,311–15,322. https://doi.org/10.1029/96JA01274

Fukushima, N., & Kamide, Y. (1973). Partial ring current models for worldwide geomagnetic disturbances. *Reviews of Geophysics*, *11*(4), 795–853. https://doi.org/10.1029/RG011i004p00795

Gonzalez, W. D., Joselyn, J. A., Kamide, Y., Kroehl, H. W., Rostoker, G., Tsurutani, B. T., & Vasyliunas, V. (1994). What is a geomagnetic storm. *Journal of Geophysical Research*, *99*(A4), 5771–5792. https://doi.org/10.1029/93JA02867

Gonzalez, W. D., & Tsurutani, B. T. (1987). Criteria of interplanetary parameters causing intense magnetic storms (Dst < −100 nT). *Planetary and Space Science*, *35*(9), 1101–1109. https://doi.org/10.1016/0032-0633(87)90015-8

Greenwald, R. A., Baker, K. B., Ruohoniemi, J. M., Dudeney, J. R., Pinnock, M., Mattin, N., et al. (1990). Simultaneous conjugate observations of dynamic variations in high-latitude dayside convection due to changes in IMF B_y. *Journal of Geophysical Research*, *95*(A6), 8057–8072. https://doi.org/10.1029/JA095iA06p08057

Grocott, A., & Milan, S. E. (2014). The influence of IMF clock angle timescales on the morphology of ionospheric convection. *Journal of Geophysical Research: Space Physics*, *119*, 5861–5876. https://doi.org/10.1002/2014JA020136

Grocott, A., Milan, S. E., Sato, N., Wild, J. A., Yeoman, T. K., & Yukimatu, A. S. (2010). Superposed epoch analysis of the ionospheric convection evolution during substorms: IMF B_Y dependence. *Journal of Geophysical Research*, *115*, A00I06. https://doi.org/10.1029/2010JA015728

Grocott, A., Yeoman, T. K., Milan, S. E., Amm, O., Frey, H. U., Juusola, L., et al. (2007). Multi-scale observations of magnetotail flux transport during IMF-northward non-substorm intervals. *Annales de Geophysique*, *25*(7), 1709–1720. https://doi.org/10.5194/angeo-25-1709-2007

Hamilton, D. C., Gloeckler, G., Ipavich, F. M., Stüdemann, W., Wilken, B., & Kremser, G. (1986). Ring current development during the great geomagnetic storm of February 1986. *Journal of Geophysical Research*, *93*(A12), 14,343–14,355.

Heelis, R. A. (1984). The effects of interplanetary magnetic field orientation on dayside high-latitude ionospheric convection. *Journal of Geophysical Research*, *89*(A5), 2873–2880. https://doi.org/10.1029/JA089iA05p02873

Iijima, T., & Potemra, T. A. (1976). The amplitude distribution of field aligned currents at northern high latitudes observed by Triad. *Journal of Geophysical Research*, *81*(13), 2165–2174. https://doi.org/10.1029/JA081i013p02165

Iyemori, T., Araki, T., Kamei, T., & Takeda, M. (1992). Mid-latitude geomagnetic indices ASY and SYM (provisional) No. 1 1989, Data Anal. Center for Geomagn. and Space Magn., Kyoto Univ., Kyoto, Japan.

Kawasaki, K., & Akasofu, S.-I. (1971). Low-latitude DS component of geomagnetic storm field. *Journal of Geophysical Research*, *76*(10), 2396–2405. https://doi.org/10.1029/JA076i010p02396

Kumar, S., Veenadhari, B., Tulasi Ram, S., Selvakumaran, R., Mukherjee, S., Singh, R., & Kadam, B. D. (2015). Estimation of interplanetary electric field conditions for historical geomagnetic storms. *Journal of Geophysical Research: Space Physics*, *120*, 7307–7317. https://doi.org/10.1002/2015JA021661

Li, H., Wang, C., & Kan, J. R. (2011). Contribution of the partial ring current to the SYMH index during magnetic storms. *Journal of Geophysical Research*, *116*, A11222. https://doi.org/10.1029/2011JA016886

Liemohn, M. W., Kozyra, J. U., Clauer, C. R., & Ridley, A. J. (2001). Computational analysis of the near-Earth magnetospheric current system during two-phase decay storms. *Journal of Geophysical Research*, *106*(A12), 29,531–29,542. https://doi.org/10.1029/2001JA000045

Liemohn, M. W., Kozyra, J. U., Jordanova, V. K., Khazanov, G. V., Thomsen, M. F., & Cayton, T. E. (1999). Analysis of early phase ring current recovery mechanisms during geomagnetic storms. *Geophysical Research Letters*, *26*(18), 2845–2848. https://doi.org/10.1029/1999GL900611

Liemohn, M. W., Kozyra, J. U., Thomsen, M. F., Roeder, J. L., Lu, G., Borovsky, J. E., & Cayton, T. E. (2001). Dominant role of the asymmetric ring current in producing the stormtime *Dst*. *Journal of Geophysical Research*, *106*(A6), 10,883–10,904. https://doi.org/10.1029/2000JA000326

Lopez, R. E., Lyon, J. G., Mitchell, E., Bruntz, R., Merkin, V. G., Brogl, S., et al. (2009). Why doesn't the ring current injection rate saturate? *Journal of Geophysical Research*, *114*, A02204. https://doi.org/10.1029/2008JA013141

Milan, S. E., Grocott, A., & Hubert, B. (2010). A superposed epoch analysis of auroral evolution during substorms: Local time of onset region. *Journal of Geophysical Research*, *115*, A00I04. https://doi.org/10.1029/2010JA015663

Milan, S. E., Wild, J. A., Grocott, A., & Draper, N. C. (2006). Space- and ground-based investigations of solar wind magnetosphere ionosphere coupling. *Advances in Space Research*, *38*(8), 1671–1677. https://doi.org/10.1016/j.asr.2005.08.009

Mitchell, E. J., Fok, M.-C. H., Lopez, R. E., & Lyon, J. G. (2013). Simulated ring current response during periods of dawn-dusk oriented interplanetary magnetic field (By). *Journal of Geophysical Research: Space Physics*, *118*, 2228–2243. https://doi.org/10.1002/jgra.50269

Miyoshi, Y., & Kataoka, R. (2005). Ring current ions and radiation belt electrons during geomagnetic storms driven by coronal mass ejections and corotating interaction regions. *Geophysical Research Letters*, *32*, L21105. https://doi.org/10.1029/2005GL024590

Murr, D. L., & Hughes, W. J. (2007). The coherence between the IMF and high-latitude ionospheric flows: The dayside magnetosphere-ionosphere low-pass filter. *Journal of Atmospheric and Terrestrial Physics*, *69*(3), 223–233. https://doi.org/10.1016/j.jastp.2006.07.019

Nopper, R. W., & Carovillano, R. L. (1978). Polar-equatorial coupling during magnetically active periods. *Geophysical Research Letters*, *5*(8), 699–702. https://doi.org/10.1029/GL005i008p00699

Ruohoniemi, J. M., & Baker, K. B. (1998). Large-scale imaging of high-latitude convection with Super Dual Auroral Radar Network HF radar observations. *Journal of Geophysical Research*, *103*(A9), 20,797–20,811. https://doi.org/10.1029/98JA01288

Ruohoniemi, J. M., & Greenwald, R. A. (2005). Dependencies of high-latitude plasma convection: Consideration of interplanetary magnetic field, seasonal, and universal time factors in statistical patterns. *Journal of Geophysical Research*, *110*, A09204. https://doi.org/10.1029/2004JA010815

Russell, C. T., Luhmann, J. G., & Lu, G. (2001). Nonlinear response of the polar ionosphere to large values of the interplanetary electric field. *Journal of Geophysical Research*, *106*(A9), 18,495–18,504. https://doi.org/10.1029/2001JA900053

Saunders, M. A. (1989). Origin of the cusp Birkeland currents. *Geophysical Research Letters*, *16*(2), 151–154. https://doi.org/10.1029/GL016i002p00151

Saunders, M. A., Freeman, M. P., Southwood, D. J., Cowley, S. W. H., Lockwood, M., Samson, J. C., et al. (1992). Dayside ionospheric convection changes in response to long-period interplanetary magnetic field oscillations: Determination of the ionospheric phase velocity. *Journal of Geophysical Research*, *97*(A12), 19,373–19,380. https://doi.org/10.1029/92JA01383

Shepherd, S. G., & Ruohoniemi, J. M. (2000). Electrostatic potential patterns in the high latitude ionosphere constrained by SuperDARN measurements. *Journal of Geophysical Research*, *105*(A10), 23,005–23,014. https://doi.org/10.1029/2000JA000171

Shi, Y., Zesta, E., Lyons, L. R., Yumoto, K., & Kitamura, K. (2006). Statistical study of effect of solar wind dynamic pressure enhancements on dawn to dusk ring current asymmetry. *Journal of Geophysical Research*, *111*, A10216. https://doi.org/10.1029/2005JA011532

Siscoe, G., Raeder, J., & Ridley, A. J. (2004). Transpolar potential saturation models compared. *Journal of Geophysical Research*, *109*, A09203. https://doi.org/10.1029/2003JA010318

Sugiura, M., & Chapman, S. (1960). The average morphology of geomagnetic storms with sudden commencement. *Abhandl. Akad. Wiss. Goettingen Math. Physik. Kl.*, *4*, 51–53.

Sugiura, M., & Kamei, T. (1991). Equatorial Dst index 1957–1986, IAGA Bull., 40, ISGI Pub., Office, Saint-Maur-des-Fossess, France.

Tanaka, T. (1995). Generation mechanisms for magnetosphere-ionosphere current systems deduced from a three-dimensional MHD simulation of the solar wind-magnetosphere ionosphere coupling processes. *Journal of Geophysical Research*, *100*(A7), 12,057–12,074. https://doi.org/10.1029/95JA00419

Tanaka, T. (2007). Magnetosphere–ionosphere convection as a compound system. *Space Science Reviews*, *133*, 1–72. https://doi.org/10.1007/s11214-007-9168-4

Tsuji, Y., Shinbori, A., Kikuchi, T., & Nagatsuma, T. (2012). Magnetic latitude and local time distributions of ionospheric currents during a geomagnetic storm. *Journal of Geophysical Research*, *117*, A07318. https://doi.org/10.1029/2012JA017566

Tsurutani, B. T., Gonzalez, W. D., Tang, F., Akasofu, S.-I., & Smith, E. J. (1988). Origin of interplanetary southward magnetic field responsible for major magnetic storms near solar maximum 1978–1979. *Journal of Geophysical Research*, *93*(A8), 8519–8531. https://doi.org/10.1029/JA093iA08p08519

Tsyganenko, N. A., & Sitnov, M. I. (2005). Modeling the dynamics of the inner magnetosphere during strong geomagnetic storms. *Journal of Geophysical Research*, *110*, A03208. https://doi.org/10.1029/2004JA010798

Tulasi Ram, S., Nilam, B., Balan, N., Zhang, Q., Shiokawa, K., Chakrabarty, D., et al. (2019). Three different episodes of prompt equatorial electric field perturbations under steady southward IMF Bz during St. Patrick's Day storm. *Journal of Geophysical Research: Space Physics*, *124*, 10,428–10,443. https://doi.org/10.1029/2019JA027069

Turner, N. E., Baker, D. N., Pulkkinen, T. I., & McPherron, R. L. (2000). Evaluation of the tail current contribution to Dst. *Journal of Geophysical Research*, *105*(A3), 5431–5439. https://doi.org/10.1029/1999JA000248

Veenadhari, B., Kikuchi, T., Kumar, S., Ram, S. T., Chakrabarty, D., Ebihara, Y., & Reeves, G. D. (2019). Signatures of substorm related overshielding electric field at equatorial latitudes under steady southward IMF Bz during main phase of magnetic storm. *Advances in Space Science*, *64*(10), 1975–1988. https://doi.org/10.1016/j.asr.2019.04.001

Weimer, D. R. (2001). Maps of ionospheric field-aligned currents as a function of the interplanetary magnetic field derived from Dynamics Explorer 2 data. *Journal of Geophysical Research*, *106*(A7), 12,889–12,902. https://doi.org/10.1029/2000JA000295

Weygand, J. M., & McPherron, R. L. (2006). Dependence of ring current asymmetry on storm phase. *Journal of Geophysical Research*, *111*, A11221. https://doi.org/10.1029/2006JA011808

Yu, Y., Ridley, A. J., Welling, D. T., & Tóth, G. (2010). Including gap region field-aligned currents and magnetospheric currents in the MHD calculation of ground-based magnetic field perturbations. *Journal of Geophysical Research*, *115*, A08207. https://doi.org/10.1029/2009JA014869

Zhao, H., Li, X., Baker, D. N., Fennell, J. F., Blake, J. B., Larsen, B. A., et al. (2015). The evolution of ring current ion energy density and energy content during geomagnetic storms based on Van Allen Probes measurements. *Journal of Geophysical Research: Space Physics*, *120*, 7493–7511. https://doi.org/10.1002/2015JA021533